ARTICLE

Curved Silicon Nanowires with Ribbon-like Cross Sections by Metal-Assisted Chemical Etching

Jungkil Kim,[†,§] Young Heon Kim,[†] Suk-Ho Choi,[§] and Woo Lee[†,‡,*]

[†]Korea Research Institute of Standards and Science (KRISS), Yuseong, 305-340 Daejeon, Korea, [‡]University of Science and Technology (UST), Yuseong, 305-333 Daejeon, Korea, and [§]Department of Applied Physics, Kyung Hee University, Yongin 446-701, Korea

ABSTRACT A generic process for the preparation of curved silicon nanowires (SiNWs) with ribbon-like cross sections was developed. The present synthetic approach is based on chemical etching of (100)-oriented silicon wafers in mixture solutions of HF and H_2O_2 by using patterned thin gold films as catalyst and provides a unique opportunity for the fabrication of extended arrays of zigzag SiNWs, ultrathin straight [111] SiNWs, and curved SiNWs with controlled turning angles. On the basis of our experiments performed under various etching conditions, the factors governing the axial crystal orientation and morphology of SiNWs were systematically analyzed. We proposed a model that explains the formation of the present novel silicon nanostructures during chemical etching of silicon.

KEYWORDS: curved Si nanowires · Si nanoribbons · metal-assisted chemical etching · gold mesh · anodic aluminum oxide (AAO)

Single-crystalline silicon nanowires (SiNWs) have attracted considerable research interests due to their intriguing chemical, optoelectronic, and mechanical properties as well as technical compatibility with the industrial integrated circuit technologies. Development of simple and robust synthetic methods to control the axial crystal orientation and morphology of SiNWs will provide researchers a solid platform for thoroughly understanding physicochemical properties of nanowires and thus for exploring various state-of-the-art applications of them.[1−8] To date, various synthetic methods have been developed for SiNWs with uniform dimensions, morphologies, and crystal orientations. These include supercritical fluid-phase approach, vapor−liquid−solid (VLS) growth, reactive ion etching (RIE), metal-assisted chemical etching, *etc.*[4,9−17] Despite large synthetic advances in the past decade, enormous challenges remain to achieve fine control over the axial orientation and morphology in the fabrication of SiNWs. Herein, we report the synthesis of extended arrays of curved SiNWs with ribbon-like cross sections by metal-assisted chemical etching of (100)-oriented silicon substrates at room temperature. The key of our synthetic protocol is to employ patterned thin gold films with arrays of nanoholes as silicon etching catalyst and to induce abrupt local changes of the reactant concentrations near the reaction interface during chemical etching of silicon in aqueous mixture solutions of HF and H_2O_2. We first show that structurally well-defined zigzag SiNWs with ribbon-like cross sections can be prepared by imposing vertical gradient of etchant concentrations during chemical etching. Enabled by our synthetic protocol, we then demonstrate fabrication of ultrathin straight [111] SiNWs with a uniform ribbon-like structure and curved SiNWs with controlled turning angles for the first time. On the basis of our experimental results obtained from various etching conditions, we provide a model that explains the formations of the present novel silicon nanostructures.

To date, several SiNW fabrication methods based on metal-assisted chemical etching have been reported. One of the most intensively utilized methods is wet chemical etching of silicon substrates with a catalyst consisting of interconnected networks of metal nanoparticles (NPs) (*e.g.*, AgNPs, AuNPs, PtNPs, *etc.*) that can be deposited either by galvanic displacement from a mixture solution containing HF and metal salt or by sputter deposition.[4−6,9,18−21] However, the resulting SiNWs exhibit poor spatial ordering and broad diameter distribution due to the random networks of metal NPs with irregular shapes. As an example, recently, Chen *et al.* reported fabrication of SiNWs with various turning angles by chemical etching of (111)-oriented Si substrates in aqueous solutions composed of HF and $AgNO_3$ (an oxidant) at elevated temperatures (T = 45−75 °C), in which AgNPs formed by galvanic displacement

* Address correspondence to woolee@kriss.re.kr.

Received for review April 19, 2011 and accepted May 10, 2011.

Published online May 10, 2011
10.1021/nn2014358

© 2011 American Chemical Society

reaction act as etching catalyst.[22] The resulting zigzag SiNWs are characterized by irregular surface etch profiles, broad size distributions, and also poor 2D spatial ordering on the starting Si(111) wafer due to random downward movements of individual AgNPs along ⟨100⟩ and other crystallographic directions in the Si(111) wafer.[22] In order to overcome these problems, in the present study, we employed thin gold mesh with ordered arrays of nanoholes, which could conveniently be replicated from porous anodic aluminum oxide (AAO) (see the Methods). Utilization of patterned metal films as etching catalyst offers several distinct advantages over conventional nanoparticle-based wet etching processes in terms of control of diameter, location, and spacing of the resulting SiNWs.[23−27]

RESULTS AND DISCUSSION

Curved SiNWs and Straight SiNWs with Ribbon-like Cross Sections. We obtained vertically aligned zigzag SiNWs by two consecutive chemical etchings of Si(100) substrates (B-doped, resistivity = 1−10 Ωcm) using etchant solutions with different molar ratios of HF to H_2O_2 (ε = [HF]/[H_2O_2]) at room temperature under an unstirred solution condition (Figure 1a). The first-step etching was conducted by immersing a gold mesh-loaded Si(100) substrate into an etchant composed of 2.424 M HF and 10.572 M H_2O_2 (ε = 0.229) for 10 min, followed by dipping into 46 wt % HF solution for 10 s. Etching of silicon under the first-step condition occurred very slowly and resulted in a thin layer of spaghetti-like porous silicon nanostructures covering continuously the entire mesh surface (see Supporting Information, Figures S1 and S2). This thin porous silicon layer plays an important role for the formation of zigzag SiNWs during the subsequent second-step etching process regulating diffusion of the reactants from the bulk reservoir to the reaction interface, which will be discussed in detail below. The second-step chemical etching was carried out by immersing the resulting sample into an etchant solution composed of 24.242 M HF and 1.057 M H_2O_2 (ε = 22.935) for a desired period of time. The nanowire part formed during the second-step etching exhibited zigzag structures (Figure 1c). However, the second-step etching conducted under solution stirring conditions yielded vertically aligned straight [100] SiNWs. In addition, direct chemical etching at room temperature without performing the first etching process produced always straight [100] SiNWs, irrespective of the ratio ε = [HF]/[H_2O_2] of the etchant. Our study indicated that the etchant composition (ε) influences only on the morphology (porous *vs* nonporous) of the resulting SiNWs without affecting their axial orientations (*i.e.*, the etching directions); vertically aligned nonporous [100] SiNWs could be obtained at ε > 1.2 (Figure S3 in Supporting Information), while porous [100] SiNWs or a continuous thin layer of porous silicon could be

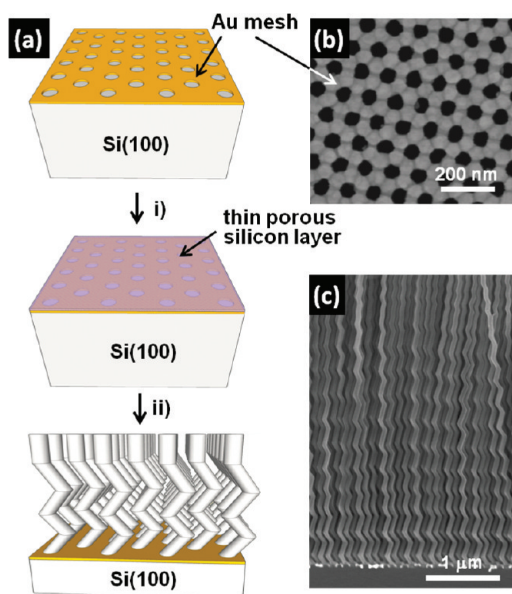

Figure 1. (a) Schematic illustration showing fabrication of zigzag SiNWs; (i) the first-step and (ii) second-step chemical etching. (b) Typical SEM micrograph of gold mesh prepared from anodic aluminum oxide (AAO). (c) Cross-sectional SEM image of Si(100) substrate after the second-step chemical etching, showing vertically aligned zigzag SiNWs.

obtained at ε < 1.2 (Figure S4). On the other hand, etching temperature (*T*) turned out to affect the etching direction, yielding tilt-aligned ultrathin SiNWs with a uniform ribbon-like structure at a temperature higher than 60 °C (*vide infra*).

Figure 2a shows stitched transmission electron microscopy (TEM) images of a typical SiNW with a zigzag nanostructure, in which nanowire parts formed during the early, middle, and last stage of the second-step chemical etching are marked with **I**, **II**, and **III**, respectively. From high-resolution TEM analysis on the respective nanowire parts (Figure 2b−d), we found the following three structural features: (i) Nanowire has initially a straight [100] orientation down to several micrometers from the original wafer surface and changes shapes into a zigzag structure, in which the wire axial orientations of straight arm parts alternate between two specific crystallographic directions on the same lattice plane. (ii) The turning angle (θ) defined by two alternating straight arms decreases with etching time at the early stage of zigzag motions but stabilizes to an almost steady-state value (*i.e.*, 70.5° formed by two crossing ⟨111⟩ directions) at the later stage. (iii) The latitudinal amplitude of spontaneous zigzag motions increases with the etching time. These three structural features were commonly observed from all of our zigzag nanowire samples.

Upon closer microscopic examination, we found that zigzag SiNWs have a unique two-dimensional (2D) geometry. They were observed to have uniform thickness (corresponding to the hole diameter (*d*) of gold mesh) along the directions perpendicular to the 2D

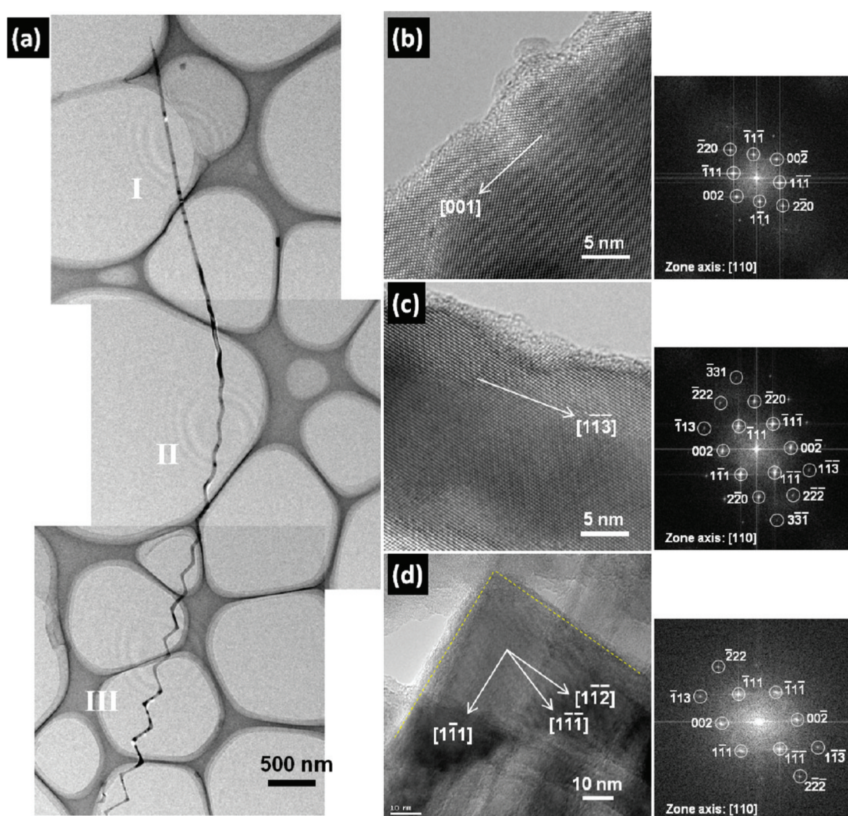

Figure 2. (a) Stitched TEM micrographs of a single SiNW obtained by metal-assisted chemical etching of Si(100) substrate, in which TEM images of the nanowire parts formed during the early, middle, and last stage of the second-step chemical etching are marked by I, II, and III, respectively. (b−d) Representative high-resolution TEM images obtained from the nanowire parts corresponding to I, II, and III, respectively. Fast Fourier transform (FFT) patterns of the TEM images shown in b−d are displayed on the right of the respective panels.

zigzag plane (see Figure 3a and its inset). On the other hand, the thickness of nanowires at the turning points (w_1) and straight arm parts (w_2) turned out to be different with $w_1 > w_2$, as indicated by the white arrows in Figure 3b. In other words, our zigzag SiNWs have a flattened elliptical shape in cross section with a ribbon-like structure. Such geometric features of zigzag nanowires are thought to be the result of uniform downward movements of 2D metal mesh along two alternate crystallographic directions with turning angles (θ) and cannot be expected from metal-assisted chemical etching of silicon utilizing randomly deposited metal NPs as catalyst. The geometric evolution of the present zigzag nanowires can be reasonably understood by simple consideration on the movement tracts of gold mesh with an ideal geometry. According to our calculation, as the turning angle (θ) decreases, wire thicknesses (w_1 and w_2) decrease systematically, and correspondingly the eccentricities (e_1 and e_2, a measure of departure of the wire cross section from circularity; see Figure S5 in Supporting Information) of elliptical wire cross sections increase (Figure 3c,d). The calculation predicted further that straight sub-10 nm thick SiNWs can be obtained by ⟨111⟩ etching of a Si(100) substrate using a catalyst gold mesh with a thickness (t) of 25 nm and a diameter (d) of 50 nm. In fact, as shown in Figure 4, we were able to demonstrate successful preparation of *ca.* 13 nm thick straight [111] SiNWs with a uniform ribbon-like structure by conducting wet chemical etching of Si(100) wafers at elevated temperatures ($T > 60$ °C), the condition under which etching proceeds along the ⟨111⟩ direction due to the enhanced injection of positive holes (h^+) into silicon, which will be discussed in detail below. The present experimental results suggest that one may conveniently prepare ultrathin silicon nanoribbons with well-defined thickness and width by employing 2D metal meshes with arrays of elongated nanoholes.

Factors Affecting the Axial Crystal Orientation and Morphology of SiNWs. The formation of the present silicon nanostructures can be explained by the etching mechanism in consideration of the microscopic electrochemical events during chemical etching of silicon. For chemical etching of a p-type silicon in a solution containing HF and H_2O_2, the cathodic current density (j) can be described by the following equation:[28−30]

$$j = -zek_c n_s c_{ox} \exp(-E_a/k_B T) \quad (1)$$

where z is the number of electrons transferred during the reaction, e is the charge of an electron, k_c is the rate constant, n_s is the electron density, c_{ox} is the H_2O_2 concentration, E_a is the activation energy for the

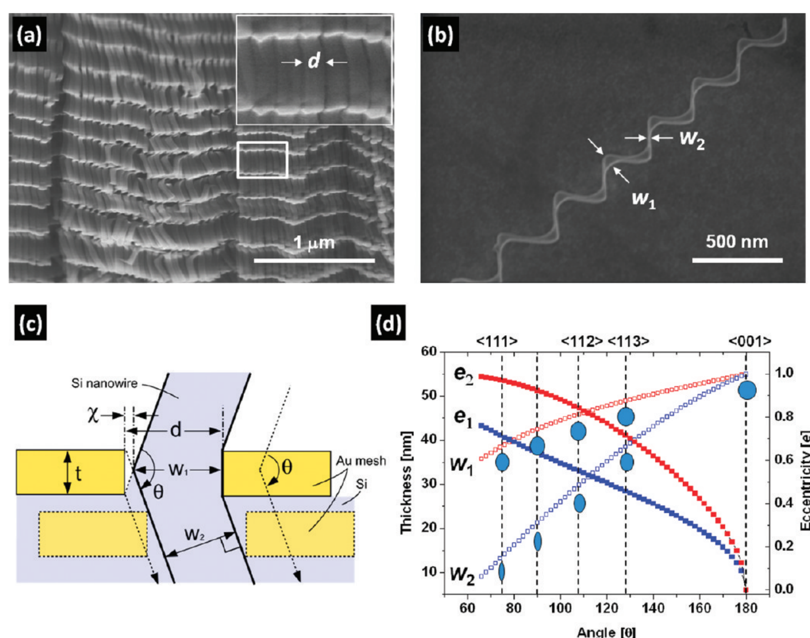

Figure 3. (a) Representative SEM image of zigzag SiNW arrays, together with a magnified SEM image of the area marked with a white rectangle as top right inset. (b) SEM image of a single zigzag SiNW, showing different wire thicknesses at the turning point (w_1) and straight arm part (w_2). (c) Schematic cross section of the etching front, together with the parameters defining the geometry of gold mesh and SiNWs; t = the thickness of gold mesh (25 nm), d = the hole diameter of gold mesh (55 nm), θ = the turning angle formed by switching of the movement tract of gold mesh (dashed arrows), $\chi = t/2\tan(\theta/2)$, $w_1 = d - \chi$, and $w_2 = (d - 2\chi)w_1\sin(\theta/2)$. (d) Graph showing the evolution of the nanowire thickness (w_n) and the eccentricity (e_n, a measure of departure of the wire cross-section from circularity; $0 < e_n < 1$) of elliptical wire cross section as a function of the turning angle (θ); $e_n = [1 - (w_n/d)^2]^{1/2}$, with n = 1, 2. The vertical dashed lines represent the angles formed by direction vectors designated on the top axis of the graph. The nanowire cross sections at the turning point and straight arm part are schematically shown on the respective dashed lines.

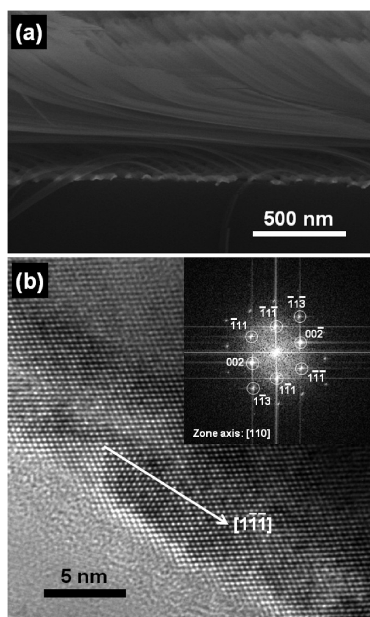

Figure 4. (a) SEM micrograph of [111] SiNWs with ribbon-like nanostructure formed by chemical etching of Si(100) substrate in an etchant solution with $\varepsilon = [HF]/[H_2O_2]$ = 22.935 at 60 °C. (b) HRTEM image of a SiNW taken from the sample shown in panel a together with corresponding fast Fourier transform (FFT) pattern as an inset.

cathodic reaction, k_B is the Boltzmann constant, and T is the absolute temperature. In metal-assisted chemical etching of silicon, a metal acts as a microscopic cathode withdrawing electrons from the underlying silicon (*i.e.*, injection of positive holes (h^+) into valence band of silicon) through the metal–silicon electrical junction and also as a catalyst for the reduction of the oxidant (*i.e.*, $H_2O_2 + 2H^+ + 2e^- \rightarrow 2H_2O$) lowering the activation energy E_a in eq 1.[9,31,32] As a consequence of this microscopic redox process, silicon contacting with a metal undergoes local oxidative dissolution in a solution containing HF (*i.e.*, $Si + h^+_{VB} + 6F^- \rightarrow SiF_6^{2-} + 3e^-_{CB}$), maintaining a metal–silicon junction and thus enabling continued movement of the etching front (*i.e.*, metal/silicon interface). In other words, the movement of the etching front is a result of the interplay between the oxidation of silicon *via* the injection of positive holes (h^+) and the removal of oxidized silicon atoms by HF through cleavage of their back bonds.[27] Since generation of holes (h^+) is positively correlated with the catalytic decomposition of H_2O_2 on the metal surface, the amount of holes (h^+) that can be injected into silicon would increase with H_2O_2 concentration (c_{ox}) or temperature (T) (*i.e.*, $[h^+] \propto$ cathodic current (j)). Accordingly, for an etchant solution composed of low relative H_2O_2 concentration (*e.g.*, $\varepsilon > 1.2$), generation of positive hole (h^+) at low temperature will be limited, and thus hole (h^+) injection into silicon will be localized at the least compact (100) plane with the fewest silicon back bonds to break, resulting in etching along the

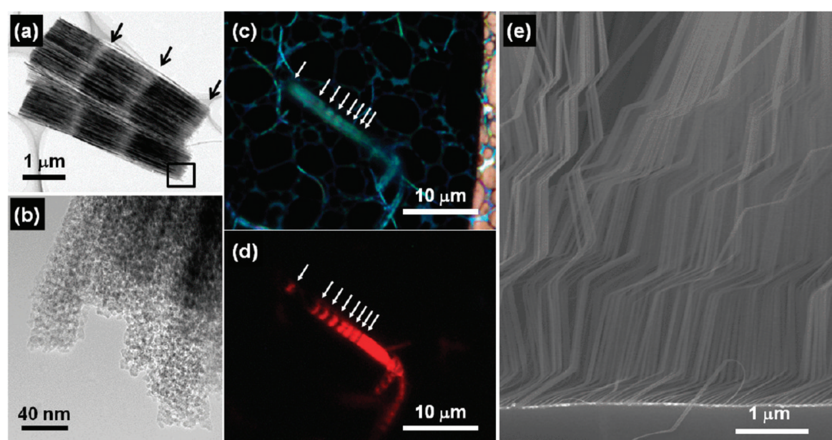

Figure 5. (a) TEM image of porosity modulated SiNWs formed by the second-step chemical etching in an etchant with ε = 2.293; SiNWs found to be easily broken at the porous segments, which are indicated by the black arrows. (b) TEM image obtained from porous region of SiNWs (the area marked by a black rectangle in panel a). (c,d) Optical microscopy images of a bundle of porosity modulated SiNWs on a Cu grid, in which porous segments are indicated by white arrows; (c) bright-field and (d) fluorescence image (excitation: a 100 W Hg lamp with a 330−385 nm band-pass filter). (e) Cross-section SEM image of Si(100) substrate etched in sequence at room temperature by using two separate etchant solutions with ε_1 = 22.935 and ε_2 = 2.293, showing curved SiNWs with controlled turning angles.

⟨100⟩ direction (see Figure S3 in Supporting Information). At high temperature, on the other hand, the amount of the generated holes (h^+) is expected to be increased due to the enhanced catalytic decomposition of H_2O_2 and also to the thermally activated carrier (h^+) injection.[27,33] In this case, silicon atoms of more compact crystal planes with higher density of silicon back bonds become labile to the oxidation, resulting in etching along non-⟨100⟩ directions, as shown in Figure 4. For etchant solutions with high relative H_2O_2 concentration (*e.g.*, $\varepsilon < 1.2$), generation of positive holes (h^+) is favored. However, removal of oxidized silicon will take place very slowly in the least compact (100) plane because HF is not readily available. In this case, an extra amount of holes (h^+) that are not consumed by oxidative dissolution of silicon can readily diffuse away from the etching front to the lattice defects and dopant sites (pore nucleation sites) on the surface of the already formed SiNWs,[5,9,24,27,34−36] resulting in vertically aligned porous [100] SiNWs (Figure S4) or even spaghetti-like porous silicon nanostructures as observed from the sample formed by the first-step chemical etching (Figures S1 and S2).

Origin of Spontaneous Formation of Zigzag SiNWs. We believe that diffusion-controlled chemical etching of silicon is mainly responsible for the formation of zigzag SiNWs during the second-step chemical etching. The continuous thin layer of porous silicon formed on the entire mesh surface by the first-step etching plays a key role not only for imposing vertical gradients of etchant concentrations but also for regulating diffusion of the reactants from the bulk reservoir to the reaction interface. As discussed above, the amount of holes (h^+) injected into silicon is proportional to the cathodic current (j), which is associated with catalytic decomposition of H_2O_2 at the metal surface. Under an unstirred solution condition with a large excess of HF, the following consecutive events could take place at the etching front. Chemical etching will quickly deplete H_2O_2 near the etching front, accompanying a sharp increase in cathodic current (j), and establishes a large concentration gradient of H_2O_2 along the direction perpendicular to the reaction interface. Depletion of H_2O_2 (*i.e.*, decrease in c_{ox} in eq 1) at the etching front will in turn result in retardation of etching reaction and thus to a decrease in cathodic current (j). At this stage, a new cycle will begin by the influx of H_2O_2 due to the vertical diffusion of the etchant. Iteration of the cycle corresponds to the periodic oscillations of cathodic current (j) during the second-step chemical etching. We think that a consequence of periodic oscillations of cathodic current (j) is switching of the etching directions, that is, etchings along the vertical ⟨100⟩ direction at low j and the slanted non-⟨100⟩ directions at high j. In each diffusion cycle, the concentration difference of H_2O_2 between the bulk etchant reservoir and the etching front will be proportional to the diffusion length of the etchant, that is, the etching time. Correspondingly, oscillating cathodic current (j) may be a sinusoidal function of time, of which amplitude increases with time at the early stage of etching, but stabilizes to a certain value at the later stage. This would explain the observed evolutions of both the latitudinal zigzag amplitude and the turning angle (θ) in zigzag SiNWs as a function of etching time (Figure 2a).

The present diffusion-controlled periodic local variations of etchant concentrations near the etching front could be supported by our control etching experiments performed at room temperature by using etchant solutions composed of low relative HF concentration (*e.g.*, ε = 2.293−4.586). The second-step chemical etchings of Si(100) substrates did not yield zigzag SiNWs but produced porosity modulated straight [100] SiNWs, in which optically active porous nanowire

segments are sandwiched between two nonporous segments (Figure 5a−d).[6] For the solution conditions employed, one may expect that HF, rather than H_2O_2, can completely be depleted by etching reaction, resulting in porosification of SiNWs due to the available holes (h^+), provided that fresh reactants are not replenished from the bulk reservoir to the reaction interface. Accordingly, formation of porosity modulated SiNWs in our control experiments undoubtedly manifests diffusion-controlled oscillations of the reactant concentrations at the reaction interface during our second-step chemical etching process. Our experiments further reveal that switching of the etching direction at room temperature can be triggered by abrupt local change of H_2O_2 concentration at the reaction interface. In fact, we could demonstrate fabrication of curved SiNWs with controlled turning angles by chemical etching of Si(100) in sequence by using two separate etchant solutions of different [HF]/[H_2O_2] ratios (*e.g.*, ε_1 = 22.935 and ε_2 = 2.293) (see Figure 5e).

CONCLUSION

In summary, we have shown that chemical etching of Si(100) substrate utilizing a patterned thin film of gold as catalyst can be successfully implemented to fabricate extended arrays of silicon nanowires (SiNWs) with controlled axial orientations and morphologies, demonstrating fabrication of structurally well-defined zigzag SiNWs, ultrathin straight [111] SiNWs, and curved SiNWs with controlled turning angles. From our systematic experiments performed under various etching conditions, we found that the axial crystal orientation and morphology of SiNWs are dictated by delicate interplay between the injection of positive holes (h^+) into the valence band of silicon, which is associated with the catalytic reduction of H_2O_2 on the gold surface, and removal of oxidized silicon by HF. In addition, we also found that abrupt local change of reactant concentrations at the reaction interface may trigger switching of etching direction even at room temperature. We provided a phenomenological model that may explain the formation of the present silicon nanostructures. Our results are expected not only to provide a viable mechanistic insight into metal-assisted chemical etching of silicon but also to pave the way for controlled synthesis of SiNWs for advanced applications.

METHODS

Pretreatment of Si Wafers. The (100)-oriented p-Si wafers (B-doped, ρ = 1−10 Ωcm) were cleaned by using either an RCA solution ($NH_3 \cdot H_2O/H_2O_2/H_2O$, v/v/v = 1/1/5) or a Piranha solution (98% H_2SO_4/30% H_2O_2, v/v = 4/1) and then thoroughly rinsed by copious amounts of deionized (DI) water prior to use.

Preparation of Porous Anodic Alumina. Self-ordered nanoporous Al_2O_3 membranes were prepared by anodization of surface finished aluminum. In brief, aluminum sheets (Goodfellow, 99.999%, typical diameter = 2 cm) were anodized under a regulated cell voltage of 40 V using 0.3 M $H_2C_2O_4$ as an electrolyte for 24 h by using an electrochemical cell equipped with a cooling stage that is in thermal contact with the aluminum substrate to remove the reaction heat.[37] After anodization, the aluminum substrate was removed by using an aqueous mixture solution containing 3.4 g of $CuCl_2 \cdot 2H_2O$, 50 mL of 38 wt % HCl, and 100 mL of DI water. Subsequently, the barrier oxide layer at the bottom of the pores was removed by using 5 wt % H_3PO_4 (32 °C). The membranes used for the present study had nominal pore diameters of 55 nm and contained 1×10^{10} pores per cm^2 of membrane surface area.

Fabrication of Au Mesh. Fabrication of gold mesh was accomplished by modifying the method reported previously (see Figure S6 in Supporting Information).[27,38] In brief, a 25 nm thick Au film was deposited onto the bottom surface of the AAO membrane in a sputter coater (208HR, Cressington, U.K.), equipped with a high-resolution thickness monitor (MTM-20, Cressington, U.K.). Deposition of metal was carried out with a rotating sample stage (rpm = 100) that was oriented at a glancing angle of *ca.* 10° with respect to the sputter source in order to minimize the deposition of metal on the pore wall surface of AAO. The resulting Au-coated AAO membrane was floated on the surface of 1 M NaOH solution to remove the oxide membrane. After that, solution neutralization was carried out by replacing the oxide etching solution with DI water. A 25 nm thick Au mesh (typical diameter = 1.6 cm) remained floating on the surface of aqueous solution and could be conveniently transferred onto substrates of choice without any structural disintegrations. The structure of Au mesh is characterized by a hexagonal arrangement of nanoholes, of which pitch distance corresponds to the interpore distance (D_{int} = 100 nm) of the AAO membrane. On the other hand, the edges of nanoholes at the bottom side of the metal mesh are contaminated with loosely connected gold particles, which are originated from the metal deposited into the pore walls of oxide nanopores during the sputter deposition process. Since individual gold nanoparticles can also participate in the silicon etching reaction resulting in irregular etched profiles, we removed them from the bottom side of the gold mesh by floating the free-standing gold mesh on the surface of a diluted aqua regia solution for 10 s. After solution neutralization with DI water, the resulting gold mesh was transferred onto the polished surface of silicon substrate. Subsequently, the sample was dried in air to remove the residual amount of water from the interface between the metal mesh and the underlying silicon substrate.

Microscopic Characterization. A Hitachi S-4800 field emission scanning electron microscope (FE-SEM) was employed for the morphological characterization of the samples. The samples were mechanically cleaved for the cross-sectional SEM investigations. The crystallographic orientation of the SiNWs were investigated by a transmission electron microscope (TEM, Tecnai F30, FEI, USA) operated at a primary beam energy of 300 kV. To prepare specimens for TEM investigation, the surface of an etched Si substrate was scraped using a razor blade, and SiNWs in the scrapings were collected and dispersed in absolute ethanol. A drop of the resulting suspension solution was placed on a carbon-coated Cu grid. Optical microscopy investigation of porosity modulated barcode-type nanowires was performed by using an Olympus BX 51 inverted microscope equipped with a bright-field reflectance filter set using a 150× oil immersion lens (NA = 1.3). A 100 W Hg lamp with a 330−380 nm band-pass filter was used for excitation.

Acknowledgment. This work was supported by Future-based Technology Development Program (Nano Fields) through the National Research Foundation of Korea (NRF) funded by the Ministry of Education, Science and Technology (Grant No. 20100029332), and in part by the Korea Research Council of Fundamental Science and Technology. The authors wish to thank J.C. Kim for his support on the preparation of porous anodic alumina. W.L. thanks H.S. Jung for her encouraging discussion and support.

ARTICLE

Supporting Information Available: Schematic experimental procedure for the preparation of patterned gold film with ordered arrays of nanoholes, electron micrographs of vertically aligned [100] SiNWs, porous [100] SiNWs, representative SEM micrographs showing a thin layer of porous silicon nanostructure formed by the first-step chemical etching, and mathematical derivation of the eccentricity (e). This material is available free of charge *via* the Internet at http://pubs.acs.org.

REFERENCES AND NOTES

1. Cui, Y.; Wei, Q.; Park, H.; Lieber, C. M. Nanowire Nanosensors for Highly Sensitive and Selective Detection of Biological and Chemical Species. *Science* **2001**, *293*, 1289–1292.
2. Chan, C. K.; Peng, H.; Liu, G.; McIlwrath, K.; Zhang, X. F.; Huggins, R. A.; Cui, Y. High-Performance Lithium Battery Anodes Using Silicon Nanowires. *Nat. Nanotechnol.* **2008**, *3*, 31–35.
3. Kelzenberg, M. D.; Boettcher, S. W.; Petykiewicz, J. A.; Turner-Evans, D. B.; Putnam, M. C.; Warren, E. L.; Spurgeon, J. M.; Briggs, R. M.; Lewis, N. S.; Atwater, H. A. Enhanced Absorption and Carrier Collection in Si Wire Arrays for Photovoltaic Applications. *Nat. Mater.* **2010**, *9*, 239–244.
4. Hochbaum, A. I.; Chen, R.; Delgado, R. D.; Liang, W.; Garnett, E. C.; Najarian, M.; Majumdar, A.; Yang, P. Enhanced Thermoelectric Performance of Rough Silicon Nanowires. *Nature* **2008**, *451*, 163–167.
5. Hochbaum, A. I.; Gargas, D.; Hwang, Y. J.; Yang, P. Single Crystalline Mesoporous Silicon Nanowires. *Nano Lett.* **2009**, *9*, 3550–3554.
6. Qu, Y.; Liao, L.; Li, Y.; Zhang, H.; Huang, Y.; Duan, X. Electrically Conductive and Optically Active Porous Silicon Nanowires. *Nano Lett.* **2009**, *9*, 4539–4543.
7. Yorikawa, H.; Uchida, H.; Muramatsu, S. Energy Gap of Nanoscale Si Rods. *J. Appl. Phys.* **1996**, *79*, 3619–3621.
8. Föll, H.; Hartz, H.; Ossei-Wusu, E.; Carstensen, J.; Rienmenschneider, O. Si Nanowire Arrays as Anodes in Li Ion Batteries. *Phys. Status Solidi RRL* **2010**, *4*, 4–6.
9. Li, X.; Bohn, P. W. Metal-Assisted Chemical Etching in HF/H_2O_2 Produces Porous Silicon. *Appl. Phys. Lett.* **2000**, *77*, 2572–2574.
10. Zschech, D.; Kim, D. H.; Milenin, A. P.; Scholz, R.; Hillebrand, R.; Hawker, C. J.; Russell, T. P.; Steinhart, M.; Gösele, U. Ordered Arrays of ⟨100⟩-Oriented Silicon Nanorods by CMOS-Compatible Block Copolymer Lithography. *Nano Lett.* **2007**, *7*, 1516–1520.
11. Ma, D. D. D.; Lee, C. S.; Au, F. C. K.; Tong, S. Y.; Lee, S. T. Small-Diameter Silicon Nanowire Surfaces. *Science* **2003**, *299*, 1874–1877.
12. Schmidt, V.; Senz, S.; Gösele, U. Diameter-Dependent Growth Direction of Epitaxial Silicon Nanowires. *Nano Lett.* **2005**, *5*, 931–935.
13. Tian, B.; Xie, P.; Kempa, T. J.; Bell, D. C.; Lieber, C. M. Single-Crystalline Kinked Semiconductor Nanowire Superstructures. *Nat. Nanotechnol.* **2009**, *4*, 824–829.
14. Holmes, J. D.; Johnston, K. P.; Doty, R. C.; Korgel, B. A. Control of Thickness and Orienation of Solution-Grown Silicon Nanowires. *Science* **2000**, *287*, 1471–1473.
15. Lee, G.; Woo, Y. S.; Yang, J.-E.; Lee, D.; Kim, C.-J.; Jo, M.-H. Directionally Integrated VLS Nanowire Growth in a Local Temperature Gradient. *Angew. Chem., Int. Ed.* **2009**, *48*, 7366–7370.
16. Peng, K.; Huang, Z.; Zhu, J. Fabrication of Large-Area Silicon Nanowire p−n Junction Diode Arrays. *Adv. Mater.* **2004**, *16*, 73–76.
17. Walavalkar, S. S.; Hofmann, C. E.; Homyk, A. P.; Henry, M. D.; Atwater, H. A.; Scherer, A. Tunable Visible and Near-IR Emission from Sub-10 nm Etched Single-Crystal Si Nanopillars. *Nano Lett.* **2010**, *10*, 4423–4428.
18. Peng, K.; Lu, A.; Zhang, R.; Lee, S.-T. Motility of Metal Nanoparticles in Silicon and Induced Anisotropic Silicon Etching. *Adv. Funct. Mater.* **2008**, *18*, 3026–3035.
19. Peng, K.; Wu, Y.; Fang, H.; Zhong, X.; Xu, Y.; Zhu, J. Uniform, Axial-Orientation Alignment of One-Dimensional Single-Crystal Silicon Nanostructure Arrays. *Angew. Chem., Int. Ed.* **2005**, *44*, 2737–3742.
20. Fang, H.; Wu, Y.; Zhao, J.; Zhu, J. Silver Catalysis in the Fabrication of Silicon Nanowire Arrays. *Nanotechnology* **2006**, *17*, 3768–3774.
21. Zhang, M.-L.; Peng, K.-Q.; Fan, X.; Jie, J.-S.; Zhang, R.-Q.; Lee, S.-T.; Wong, N.-B. Preparation of Large-Area Uniform Silicon Nanowires Arrays through Metal-Assisted Chemical Etching. *J. Phys. Chem. C* **2008**, *112*, 4444–4450.
22. Chen, H.; Wang, H.; Zhang, X.-H.; Lee, C.-S.; Lee, S.-T. Wafer-Scale Synthesis of Single-Crystal Zigzag Silicon Nanowire Arrays with Controlled Turning Angle. *Nano Lett.* **2010**, *10*, 864–868.
23. Chang, S.-W.; Chuang, V. P.; Boles, S. T.; Ross, C. A.; Thompson, C. V. Densely Packed Arrays of Ultra-High-Aspect-Ratio Silicon Nanowires Fabricated Using Block-Copolymer Lithography and Metal-Assisted Etching. *Adv. Funct. Mater.* **2009**, *19*, 2495–2500.
24. Chern, W.; Hsu, K.; Chun, I. S.; Azeredo, B. P. d.; Ahmed, N.; Kim, K.-H.; Zuo, J.-m.; Fang, N.; Ferreira, P.; Li, X. Nonlithographic Patterning and Metal-Assisted Chemical Etching for Manufacturing of Tunable Light-Emitting Silicon Nanowire Arrays. *Nano Lett.* **2010**, *10*, 1582–1588.
25. Huang, Z.; Fang, H.; Zhu, J. Fabrication of Silicon Nanowire Arrays with Controlled Diameter, Length, and Density. *Adv. Mater.* **2007**, *19*, 744–748.
26. Huang, Z.; Zhang, X.; Reiche, M.; Liu, L.; Lee, W.; Shimizu, T.; Senz, S.; Gösele, U. Extended Arrays of Vertically Aligned Sub-10 nm Diameter [100] Si Nanowires by Metal-Assisted Chemical Etching. *Nano Lett.* **2008**, *8*, 3046–3051.
27. Kim, J.; Han, H.; Kim, Y. H.; Choi, S.-H.; Kim, J.-C.; Lee, W. Au/Ag Bilayered Metal Mesh as a Si Etching Catalyst for Controlled Fabrication of Si Nanowires. *ACS Nano* **2011**, *5*, 3222–3229.
28. Bertagna, V.; Plougonven, C.; Rouelle, F.; Chemla, M. p- and n-Type Silicon Electrochemical Properties in Dilute Hydrofluoric Acid Solution. *J. Electrochem. Soc.* **1996**, *143*, 3532–3538.
29. Bertagna, V.; Plougonven, C.; Rouelle, F.; Chemla, M. Kinetics of Electrochemical Corrosion of Silicon Wafers in Dilute HF Solutions. *J. Electroanal. Chem.* **1997**, *422*, 115–123.
30. Mitsugi, N.; Nagai, K. Pit Formation Induced by Copper Contamination on Silicon Surface Immersed in Dilute Hydrofluoric Acid Solution. *J. Electrochem. Soc.* **2004**, *151*, G302–G306.
31. Kooij, E. S.; Vanmaekelbergh, D. Catalysis and Pore Initiation in the Anodic Dissolution of Silicon in HF. *J. Electrochem. Soc.* **1997**, *144*, 1296–1301.
32. Xia, X. H.; Ashruf, C. M. A.; French, P. J.; Kelly, J. J. Galvanic Cell Formation in Silicon/Metal Contacts: The Effect on Silicon Surface Morphology. *Chem. Mater.* **2000**, *12*, 1671–1678.
33. Goszner, K.; Bischof, H. The Decomposition of Hydrogen Peroxide on Silver−Gold Alloys. *J. Catal.* **1974**, *32*, 175–182.
34. Cullis, A. G.; Canham, L. T.; Calcott, P. D. The Structural and Luminescence Properties of Porous Silicon. *J. Appl. Phys.* **1997**, *82*, 909–965.
35. Smith, R. L.; Collins, S. D. Porous Silicon Formation Mechanisms. *J. Appl. Phys.* **1992**, *71*, R1–R22.
36. Tsujino, K.; Matsumura, M. Helical Nanoholes Bored in Silicon by Wet Chemical Etching Using Platinum Nanoparticles as Catalyst. *Electrochem. Solid-State Lett.* **2005**, *8*, C193–C195.
37. Lee, W.; Ji, R.; Gösele, U.; Nielsch, K. Fast Fabrication of Long-Range Ordered Porous Alumina Membranes by Hard Anodization. *Nat. Mater.* **2006**, *5*, 741–747.
38. Lee, W.; Alexe, M.; Nielsch, K.; Gösele, U. Metal Membranes with Hierarchically Organized Nanotube Arrays. *Chem. Mater.* **2005**, *17*, 3325–3327.